

Excessive localized leukotriene B₄ levels dictate poor skin host defense in diabetic mice

Stephanie L. Brandt,^{1,6} Sue Wang,⁶ Naiara N. DeJani,⁶ Nathan Klopfenstein,^{1,2} Seth Winfree,⁴ Luciano Filgueiras,⁶ Brian P. McCarthy,⁵ Paul R. Territo,⁵ and C. Henrique Serezani^{1,2,3,6}

¹Department of Medicine, Division of Infectious Diseases, ² Department of Pathology, Microbiology, and Immunology, and ³Vanderbilt Institute of Infection, Immunology and Inflammation, Vanderbilt University Medical Center, Nashville, Tennessee, USA. ⁴Indiana Center for Biological Microscopy, Indianapolis, Indiana, USA. ⁵Indiana Institute for Biomedical Imaging Sciences, Department of Radiology, Indianapolis, Indiana, USA. ⁶Indiana University School of Medicine, Department of Microbiology & Immunology, Indiana University, Indianapolis, Indiana, USA.

Poorly controlled diabetes leads to comorbidities and enhanced susceptibility to infections. While the immune components involved in wound healing in diabetes have been studied, the components involved in susceptibility to skin infections remain unclear. Here, we examined the effects of the inflammatory lipid mediator leukotriene B₄ (LTB₄) signaling through its receptor B leukotriene receptor 1 (BLT1) in the progression of methicillin-resistant *Staphylococcus aureus* (MRSA) skin infection in 2 models of diabetes. Diabetic mice produced higher levels of LTB₄ in the skin, which correlated with larger nonhealing lesion areas and increased bacterial loads compared with nondiabetic mice. High LTB₄ levels were also associated with dysregulated cytokine and chemokine production, excessive neutrophil migration but impaired abscess formation, and uncontrolled collagen deposition. Both genetic deletion and topical pharmacological BLT1 antagonism restored inflammatory response and abscess formation, followed by a reduction in the bacterial load and lesion area in the diabetic mice. Macrophage depletion in diabetic mice limited LTB₄ production and improved abscess architecture and skin host defense. These data demonstrate that exaggerated LTB₄/BLT1 responses mediate a derailed inflammatory milieu that underlies poor host defense in diabetes. Prevention of LTB₄ production/actions could provide a new therapeutic strategy to restore host defense in diabetes.

Introduction

The global prevalence of diabetes is expected to increase from 171 million to 366 million by the year 2030 (1). Uncontrolled glycemia is often associated with numerous comorbidities such as increased susceptibility to infections that commonly affect the lung, urinary tract, skin, and soft tissues (2, 3). Diabetic foot ulcers are frequent targets of skin infections that take significantly longer to heal, and they often require amputation as a result of chronic or recurrent infections (4). In the US, the treatment cost of diabetic foot ulcers represents one-third of ~\$116 billion spent annually on treating complications associated with diabetes (5). Antibiotic-resistant pathogens, such as methicillin-resistant *Staphylococcus aureus* (*S. aureus*; MRSA) pose an additional risk to immunocompromised individuals due to the challenge of efficiently treating these infections. Additionally, if left untreated, skin infections may disseminate to deeper tissues and cause life-threatening infections, such as sepsis, osteomyelitis, and endocarditis (6).

S. aureus skin infections are initially controlled by tissue-resident innate immune cells, including keratinocytes and macrophages (7). These cells produce antimicrobial peptides and a variety of other inflammatory mediators, including cytokines, chemokines, metalloproteases, and lipids (7). These factors recruit and activate neutrophils and monocyte-derived macrophages to the site of infection and promote the development of an abscess (8). Abscesses are formed by live and dead neutrophils, cell debris, bacteria, fibrin, and collagen encapsulated within a fibrous material (8). *S. aureus* skin abscesses form in 12–24 hours, with most studies focused on the role of cytokines/chemokines in abscess formation. Therefore, the early inflammatory signals that initiate skin host defense are unclear. Despite our

Conflict of interest: The authors have declared that no conflict of interest exists.

Submitted: January 29, 2018

Accepted: July 26, 2018

Published: September 6, 2018

Reference information:

JCI Insight. 2018;3(17):e120220.

<https://doi.org/10.1172/jci.insight.120220>.

insight.120220.

lack of understanding of these cellular and molecular events, it is anticipated that these events must be tightly controlled to prevent poor host defense and severe tissue damage.

In response to infection, leukotriene B₄ (LTB₄) is produced within seconds to minutes via arachidonic acid metabolism by 5-lipoxygenase (5-LO) to LTA₄, which is further metabolized by the LTA₄ hydrolase (LTA4H) to LTB₄ (9). LTB₄ via its high-affinity B₂LT receptor 1 (BLT1) and low-affinity BLT2 are known phagocyte chemoattractants, and recently, we and others have shown that LTB₄ amplifies different arms of phagocyte effector function in response to various pathogens, including bacteria, fungi, and parasites (10–16). However, enhanced and sustained LTB₄ levels are associated with chronic inflammation, such as in chronic obstructive pulmonary disease (17), arthritis (18), and insulin resistance (19). Importantly, in zebrafish, overexpression of LTA4H has been shown to increase susceptibility to mycobacterium infection (20), and a gain-of-function mutation in the LTA4H locus is associated with increased susceptibility to tuberculosis infection in a human cohort from India (20). We have shown that diabetic mice have higher levels of serum LTB₄ than nondiabetic mice, which is associated with higher mortality during sepsis (21). Diabetic *Ltb4r1*^{-/-} or WT diabetic mice treated with a 5-LO inhibitor have been shown to increase survival during sepsis, concomitant with decreased systemic IL-1β, TNFα, and IL-6 (21). Therefore, inappropriate innate immune activation and production of inflammatory mediators may unbalance the chemotaxis gradients and induce tissue injury associated with reduced host defense. However, it is unclear whether overabundant and sustained LTB₄ production drives insufficient host defense and tissue damage in the skin of diabetic subjects. Here, we performed epistatic and gain-of-function experiments to determine the impact of pronounced LTB₄/BLT1 effects on both early and late events involved in the control of MRSA skin infection in diabetic mice. We demonstrate that diabetic mice produced abnormally high skin levels of LTB₄ in response to MRSA skin infection and that these LTB₄ levels dictated uncontrolled neutrophil chemotaxis, abscess formation, and insufficient bacterial clearance in diabetic mice. Importantly, treating diabetic mice daily with topical ointment containing BLT1 antagonist limited inflammation and restored host defense mechanisms, allowing for bacterial removal. These data provide a therapeutic rationale for targeting LTB₄/BLT1 as a strategy for treating MRSA skin infections in people with preexisting conditions, such as diabetes.

Results

Diabetic mice have poor infection control due to exaggerated inflammation. Initially, we evaluated differences in MRSA skin infection between diabetic and nondiabetic control animals. We induced diabetes by challenging mice with streptozotocin (STZ), and 30 days after STZ treatment, mice were subjected to MRSA skin infection. Diabetic mice developed larger lesions and had a greater bacterial load 9 days after infection, whereas nondiabetic mice were mostly healed from the infection (Figure 1, A–C). To determine whether increased susceptibility to infection is not restricted to our diabetes model, we infected diabetic NOD (dbNOD) and nondiabetic NOD mice (ctNOD). The dbNOD mice had significantly larger, nonhealing lesions compared with ctNOD mice (Supplemental Figure 1, A and B; supplemental material available online with this article; <https://doi.org/10.1172/jci.insight.120220DS1>), as well as a higher bacterial burden (Supplemental Figure 1C). Since the NOD genetic background is known to have impaired innate and adaptive immune functions (22–24), we decided to further pursue our studies using the STZ-induced diabetes model.

Next, we aimed to understand whether poor host defense was due to increased inflammatory response and/or inadequate bacterial clearance. Diabetic and nondiabetic mice were infected with heat-killed MRSA (HK-MRSA) to evaluate host activation and inflammation in the absence of bacterial growth. In both STZ-diabetic (Supplemental Figure 2A) and dbNOD (Supplemental Figure 2B) mice, HK-MRSA induced more inflammation than in the respective nondiabetic controls. Additionally, we observed more cell recruitment to the skin of STZ-diabetic mice compared with nondiabetic controls (Supplemental Figure 2, C and D). Others have reported that live bacteria are required for abscess formation (25), so it is not surprising that we did not observe abscess formation in the skin with the HK-MRSA challenge. Nonetheless, these data suggest that intrinsic differences in immune cell activation in diabetic mice may lead to poor disease outcome during an active infection, leading to inflammation-induced tissue damage in diabetic mice.

Increased local LTB₄ production is detrimental to skin host defense in diabetic mice. We have shown that diabetes is accompanied by high levels of systemic LTB₄, which causes systemic inflammation and increased mortality in a model of polymicrobial sepsis (21). During MRSA skin infection, the involvement of cytokines and chemokines are well studied; however, the role of mediators that are produced immediately (within seconds to minutes) by the host remains to be determined.

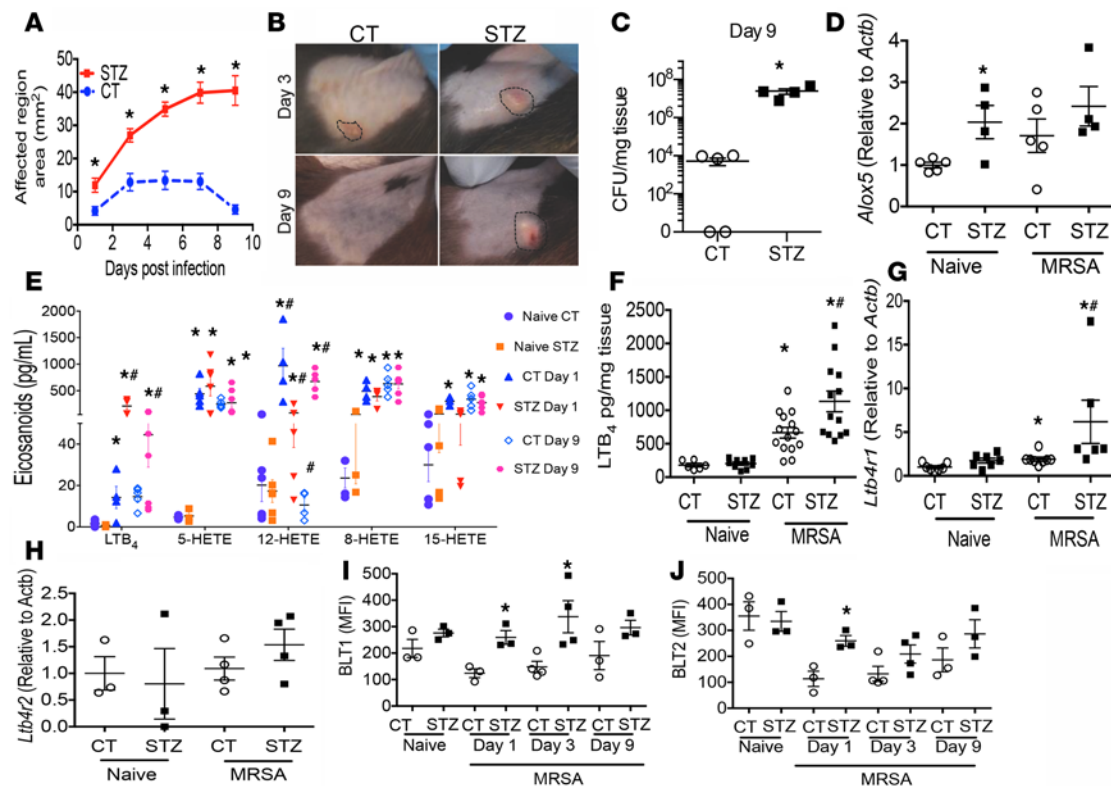


Figure 1. Increased lesion size and bacterial loads in diabetic mice correlates with higher LTB_4 levels than nondiabetic infected mice. (A) STZ-diabetic and control (CT) mice were infected s.c. with 3×10^6 CFU and infection areas were measured every other day for 9 days. Data represent mean \pm SEM ($*P < 0.05$, 2-way ANOVA with 2-way ANOVA followed by Tukey's multiple comparison corrections). (B) Photographs of CT and STZ mice at days 3 and 9 after infection. (C) Bacterial CFUs measured from skin biopsy homogenates at day 9 after infection. (D) *Alox5* mRNA expression in skin from diabetic and CT mice on day 1 after infection detected by quantitative PCR (qPCR). (E) Eicosanoids measured by mass spectrometry from skin biopsy homogenates from the naive skin and from samples taken on day 1 and 9 after infection from diabetic and nondiabetic mice. (F) LTB_4 in the skin of diabetic and nondiabetic mice at 1 day after infection and measured by EIA. (G) *Ltb4r1* mRNA expression in skin from diabetic and CT mice on day 1 after infection detected by qPCR. (H) *Ltb4r2* mRNA expression in skin from diabetic and CT mice on day 1 after infection detected by qPCR. Data are mean \pm SEM of 5–10 mice from 2–5 experiments. $*P < 0.05$ vs. naive mice. $\#P < 0.05$ vs. CT mice.

We are speculating that initial LTB_4 production may shape the innate immune response to influence the outcome of the infection. Initially, we measured the skin mRNA expression of the gene that encodes 5-LO, *Alox5*, during MRSA skin infection in both diabetic and nondiabetic mice. We detected higher basal expression of *Alox5* in the skin of diabetic mice than in the skin of nondiabetic mice; however, no difference in expression between the 2 groups was detected at day 1 after infection (Figure 1D). Since regulation of eicosanoid synthesis enzymes are tightly controlled (26), we next measured the abundance of different lipoxygenases (LOX) products, including 5-LO (LTB_4 and 5-hydroxyeicosatetraenoic acid; 5-HETE), 12-LOX (12-HETE and 15-HETE), and 8-LOX (8-HETE) by mass spectrometry (MS). Interestingly, LTB_4 was the only LOX product that was substantially increased at both days 1 and 9 after infection with MRSA in the skin of diabetic mice (Figure 1E). Elevated levels of LTB_4 in the infected skin of diabetic mice were further confirmed using enzyme immunoassay (Figure 1F). These data show a skewing toward LTB_4 production in the skin of diabetic mice during MRSA skin infection.

Uncontrolled LTB_4 /BLT1 activity drives poor host defense in diabetic mice. Since LTB_4 signals through both BLT1 and BLT2, we studied the mRNA expression levels of these receptors during MRSA infection in diabetic and nondiabetic mice. Expression of *Ltb4r1*, but not *Ltb4r2*, was higher in the skin of diabetic mice at day 1 after infection (Figure 1, G and H). BLT1 and BLT2 expression were also determined as mean fluorescence intensity (MFI) of all cells in the skin by flow cytometry (Figure 1, I and J). This suggests that BLT1 might be the predominant BLT receptor involved in detrimental LTB_4 effects in increased susceptibility to MRSA skin infection in diabetic mice.

To assess whether aberrant LTB_4 production is indeed involved in deficient skin host defense in diabetic mice, we induced diabetes in both BLT1-deficient (*Ltb4r1*^{-/-}) and 5-LO-deficient (*Alox5*^{-/-}) mice prior to

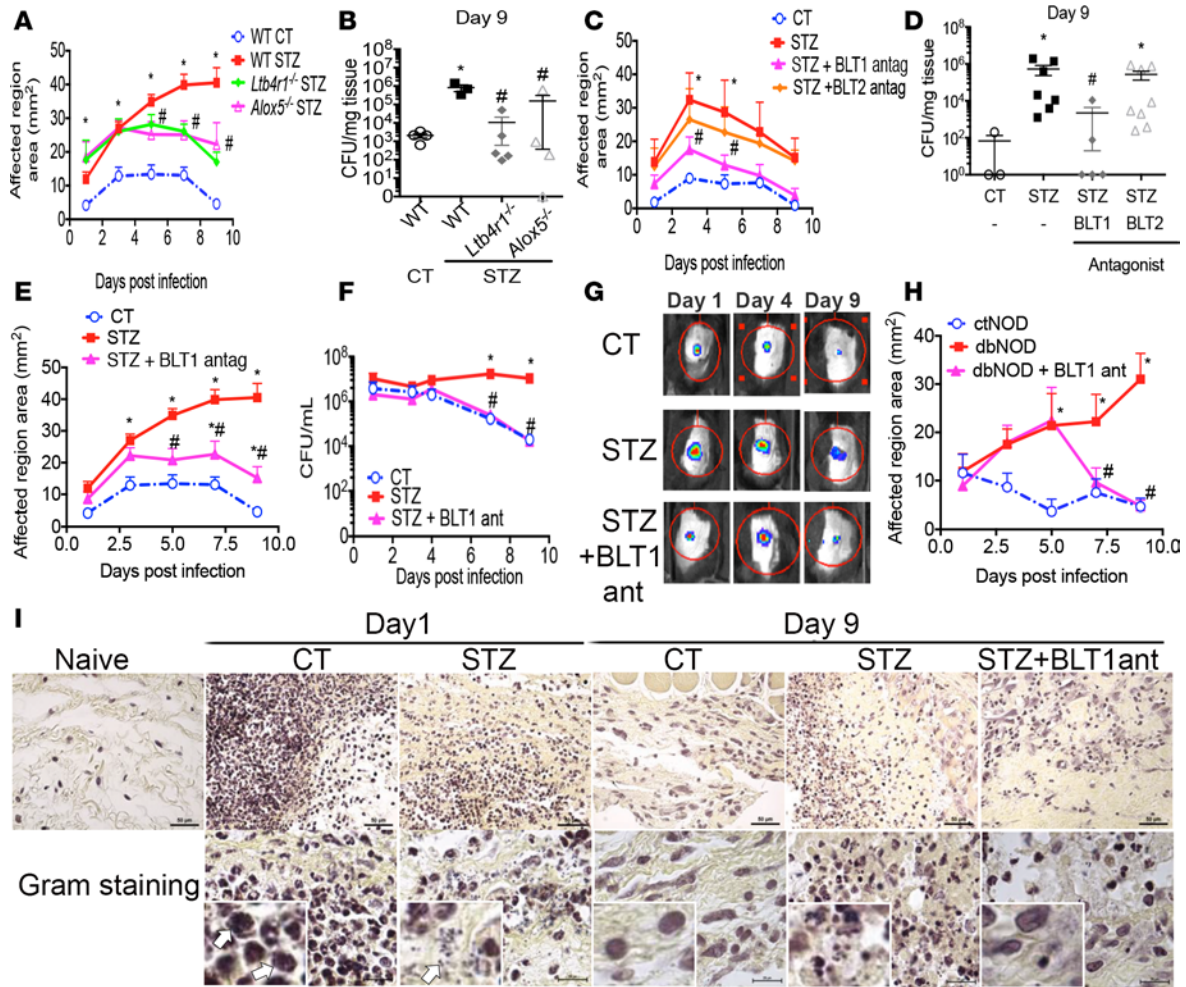


Figure 2. Inhibition of BLT1, but not BLT2, improves host defense in diabetic mice during MRSA skin infection. (A) WT CT, STZ-treated WT, STZ-treated *Alox5^{-/-}*, and STZ-treated *Ltb4r1^{-/-}* mice were infected s.c. with MRSA, and infection areas were measured for 9 days. (B) Bacterial CFUs in the skin at day 9 after infection. Data are mean ± SEM of 5–10 mice. **P* < 0.05 vs. WT CT mice. #*P* < 0.05 vs. STZ-treated WT mice. (C) CT and STZ-treated mice were infected s.c. with MRSA. STZ-treated mice were treated daily with topical ointments, vehicle-control, 0.001% BLT1 antagonist (U-75302), or 0.001% BLT2 antagonist (LY255283), and infection area was measured as in A. (D) Bacterial CFUs from mice in C at day 9 after infection. Data are mean ± SEM of 4–6 mice. **P* < 0.05 vs. CT mice. #*P* < 0.05 vs. STZ-treated mice treated with vehicle control ointment. (E) Mice were infected s.c. with bioluminescent-expressing MRSA. Infection areas were measured every other day in CT and STZ-treated mice treated daily with vehicle control or 0.001% BLT1 antagonist (U-75302) ointments. (F) Bioluminescence imaging (BLI) to quantify bacterial burden in the skin at days 1, 3, 4, 7, and 9 after infection. (G) Representative images of bioluminescent MRSA infection in control and diabetic mice that were treated or not with BLT1 antagonist scanned by BLI. (H) Lesion size of nondiabetic NOD (ctNOD) and diabetic NOD (dbNOD) mice infected with MRSA by s.c. injection. Infected dbNOD mice were treated daily with vehicle-control or 0.001% BLT1 antagonist (U-75302) ointments as in C. Data are mean ± SEM of 5–10 mice. **P* < 0.05 vs. CT mice. #*P* < 0.05 vs. STZ-treated mice treated with vehicle control. (I) Gram stains of CT and diabetic mice that were infected and treated with the BLT1 antagonist with MRSA for 1 and 9 after infection. Top panels show 100× and bottom panels show 1,000× magnification with an inset of a cropped zoomed view of 5,000× magnification. Arrows indicate bacteria.

MRSA skin infection. While diabetic WT mice were more susceptible to MRSA skin infection, diabetic *Ltb4r1^{-/-}* and *Alox5^{-/-}* mice developed smaller lesions (Figure 2A) and lower bacterial burdens (Figure 2B) than WT diabetic animals. These data demonstrate that excessive LTB₄ production and BLT1 activity are contributing to detrimental host defense in diabetic mice.

To define a role for BLT1 signaling in poor skin host defense and to determine whether blocking LTB₄ receptors could have therapeutic benefits, diabetic mice were infected with MRSA and treated daily with topical ointments containing antagonists for BLT1 (U-75302) or BLT2 (LY255283). Lesions of STZ-diabetic mice treated with a BLT1 antagonist, but not with a BLT2 antagonist, were significantly smaller than lesions in untreated STZ mice (Figure 2C). These smaller lesions correlated with lower bacterial burdens in the skin at day 9 after infection following BLT1 antagonist treatment (Figure 2D). We confirmed these findings using *in vivo* imaging system (IVIS) of bioluminescent MRSA strain in diabetic and nondiabetic mice (Figure 2E) and found that

diabetic mice were unable to eliminate bacteria, whereas diabetic mice treated with BLT1 antagonist exhibited increased bacterial clearance (Figure 2, F and G). Furthermore, BLT1 antagonist topical ointment also decreased lesion size in dbNOD mice, but not in dbNOD treated with vehicle control (Figure 2H). We next examined Gram stains of histology slides to determine whether differences in bacterial ingestion, niche location, and burden were evident between the animals. MRSA was found mostly within cells in nondiabetic mice, while a higher abundance of extracellular bacteria was observed in the skin of diabetic mice at day 1 after infection. At day 9 after infection, few to no bacteria were found in the skin of nondiabetic mice, while diabetic mice were unable to control bacterial burden. However, treatment of diabetic mice with a BLT1 antagonist promoted bacterial clearance (Figure 2I). These data show that BLT1 antagonist treatment improves host defense of diabetic mice during MRSA skin infection by improving phagocyte recruitment and antimicrobial effector functions.

Impaired abscess formation in diabetic mice. Because MRSA infections characteristically involve neutrophil recruitment and abscess formation, we investigated any differences in the morphology and architecture of the abscess between diabetic and nondiabetic mice. An abscess comprises live and dead neutrophils, macrophages, bacteria, and other immune cells that are contained by a capsule that is composed of fibrin and collagen fibers (8, 27). At day 1 after infection, nondiabetic mice showed characteristic cell recruitment and abscess formation. Tissue sections of the abscess from diabetic mice showed robust cell recruitment to the infection site; however, cells were observed in all layers of the dermis and did not form an organized abscess (Figure 3A). In contrast, infected nondiabetic mice exhibited a well-defined abscess characterized by bacteria and neutrophils inside a fibrous capsule. By H&E staining, we observed a fibrous structure surrounding the abscess in infected nondiabetic mice, but this structure was not apparent in diabetic mice (Figure 3A). We next determined whether diabetic mice had impaired capsule production or formation. Histology sections were stained with Masson's trichrome blue to label collagen (Figure 3B). While the fibrous capsule in nondiabetic mice at day 1 after MRSA skin infection showed abundant collagen, we observed irregular and exaggerated collagen deposition in the skin of diabetic mice at day 1 after MRSA skin infection (Figure 3B). Treatment of diabetic mice with BLT1 antagonist U-75302 partially restored structured abscess formation, as evidenced by more compact cell accumulations at day 9 after infection, fewer neutrophils and macrophages were found in the skin of nondiabetic mice, but diabetic mice had abundant cell numbers in the skin. Furthermore, BLT1 antagonist treatment restricted cell migration to the site of infection in diabetic mice (Figure 3A). The irregular deposition of these fibrous molecules, along with dispersed neutrophil accumulations in the skin of diabetic mice, may be associated with reduced abscess formation and consequently poor bacterial control.

The inflammatory milieu is altered in the skin of diabetic mice. Because we observed a lack of abscess organization in the skin of infected diabetic mice, we next investigated whether the chronic inflammatory diabetic milieu impairs neutrophil recruitment and migration in the infected skin. When skin biopsies were stained with a neutrophil marker (Ly6G/C) by IHC, we observed few to no neutrophils in the skin of naive mice (Figure 4A). At day 1 after MRSA skin infection, we detected an abundance of neutrophils, which were mostly organized within the abscess in the skin of nondiabetic mice (Figure 4A). Similar to our earlier findings (Figure 3A), diabetic mice had no apparent impairment in neutrophil migration to the skin but lacked an organized abscess structure (Figure 4A). BLT1 antagonist treatment of the diabetic mice both limited neutrophil recruitment and concentrated these immune cells in areas near the infection site in the skin. At day 9 after infection, whereas the skin of nondiabetic mice had few neutrophils, the skin of diabetic mice still had abundant neutrophils; this abundance was reduced with BLT1 antagonist treatment (Figure 4A).

Since neutrophils in the skin of diabetic mice during MRSA skin infection were not organized into abscesses, we next determined whether abundant LTB_4 levels in the skin of diabetic mice altered the dynamics of cell migration and directed chemotaxis at the site of infection during MRSA skin infection. MRSA-infected diabetic and nondiabetic mice with myeloid cells that expressed EGFP (Lys^{EGFP}) were treated with the BLT1 antagonist or left untreated and used for 2-photon intravital microscopy imaging. At day 1 after infection, skin flaps of anesthetized mice were imaged for 30 minutes (Figure 4B). Although we attempted to image the cells within the abscess, we did not observe any cell movement or chemotaxis (not shown). Therefore, regions located near the abscess were chosen to follow the dynamics of the neutrophils during MRSA skin infection. Neutrophils in infected nondiabetic mice formed swarm-like accumulations, whereas neutrophils in infected diabetic mice exhibited faster movement but lacked apparent direction (Figure 4C). Neutrophils in diabetic mice treated with BLT1 antagonist showed surprisingly quicker movement than neutrophils in untreated diabetic animals, and the swarm-like accumulations were partially restored. Also, lack of accumulation of myeloid cells — as evidenced

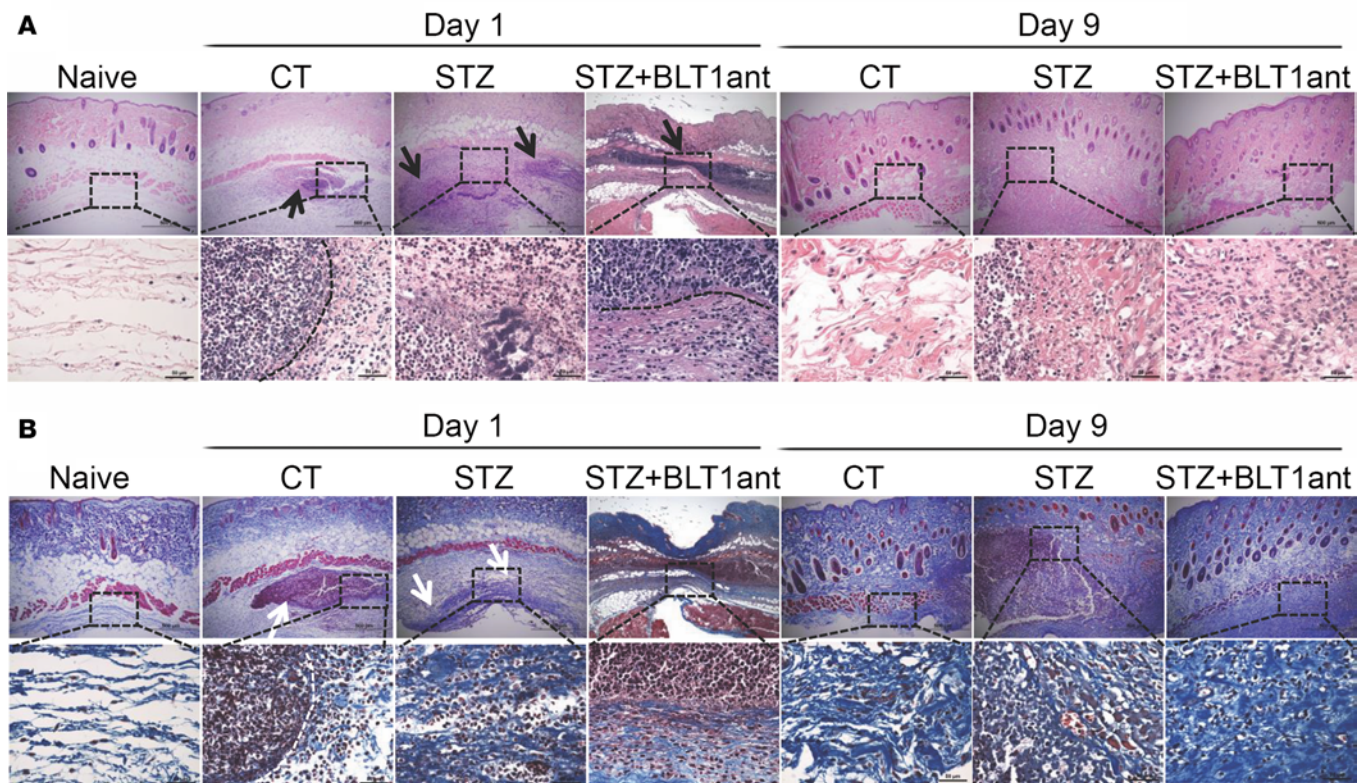


Figure 3. Diabetic mice have compromised abscess morphology. (A) CT and STZ-treated mice were infected with MRSA by s.c. injection. STZ-treated mice were treated daily with topical 0.001% BLT1 antagonist (U-75302) ointment or vehicle control, and biopsies were collected at day 1 after MRSA skin infection or from naive skin and sectioned for histology and H&E staining. The black dotted line outlines the abscess edge. Black arrows indicate cell recruitment. (B) Representative images for slides stained with Masson's trichrome blue stain of control and diabetic mice infected and treated as above. White arrows and dotted lines show abscess edge. In all circumstances, stained images are representative of 3–5 mice/group from 2–4 experiments. Top panels show 40 \times magnification, and bottom panels show 400 \times magnification.

by greater displacement of neutrophil migration in the skin of diabetic mice compared with nondiabetic mice — and BLT1 antagonist further increased the displacement of these neutrophils in diabetic mice (Figure 4C). The ratio of displacement to duration was higher in neutrophils from diabetic mice treated with BLT1 antagonist than in those from untreated diabetic mice (Figure 4C), suggesting that blockade of BLT1 in diabetic mice during MRSA skin infection allows for neutrophils to better locate bacteria and aggregate to form an abscess.

Next, we determined whether inflammatory mediators were altered in the skin of diabetic mice with BLT1 antagonist treatment and whether this correlated with the intravital microscopy observations. Skin biopsies and skin biopsy homogenates from diabetic and nondiabetic mice treated with the BLT1 antagonist or left untreated were harvest on days 1 and 9 after infection and were tested in a multiplex assay to detect multiple mediators at once (Figure 4D). Interestingly, at day 1 of infection, infection of diabetic mice induced higher levels of ICAM1, MCP3, IL-33, IL-12p70, IL-1 α , and receptor for advanced glycation end-products (RAGE). We also observed a decreased level of chemokines (CXCL1, CXCL2, MIP1 β , and CCL2), cytokines (IL-1 β), and P-selectin — all involved in neutrophil and monocyte recruitment and activation — when compared to infected-nondiabetic mice. Interestingly, BLT1 antagonist treatment in the infected diabetic mice restored the production of ICAM1, MCP3, IL-1 α , IL-33, and IL-12p70 and increased the levels of chemokines CCL2, CXCL2, and P-selectin back to the levels detected in the infected nondiabetic mice. When we studied the production of the inflammatory mediators at day 9 after infection, we observed a robustly increased production of chemokines (CXCL1, CCL2, CCL8, MCP3, MIP1 β) and P-selectin and a sustained increased of ICAM1, IL-1 α , and IL-33. At this time point, both IL-12p70 and RAGE were decreased when compared with infected nondiabetic mice (Figure 4E). Here, daily treatment of infected diabetic mice with the BLT1 antagonist for 9 days increased the levels of VEGF, IL-1 α , IL-1 β , and RAGE and decreased ICAM1, P-selectin, CXCL2, and CCL8 when compared with the skin of infected diabetic mice treated with the vehicle control (Figure 4D). The right panels confirms the heatmap representation of the

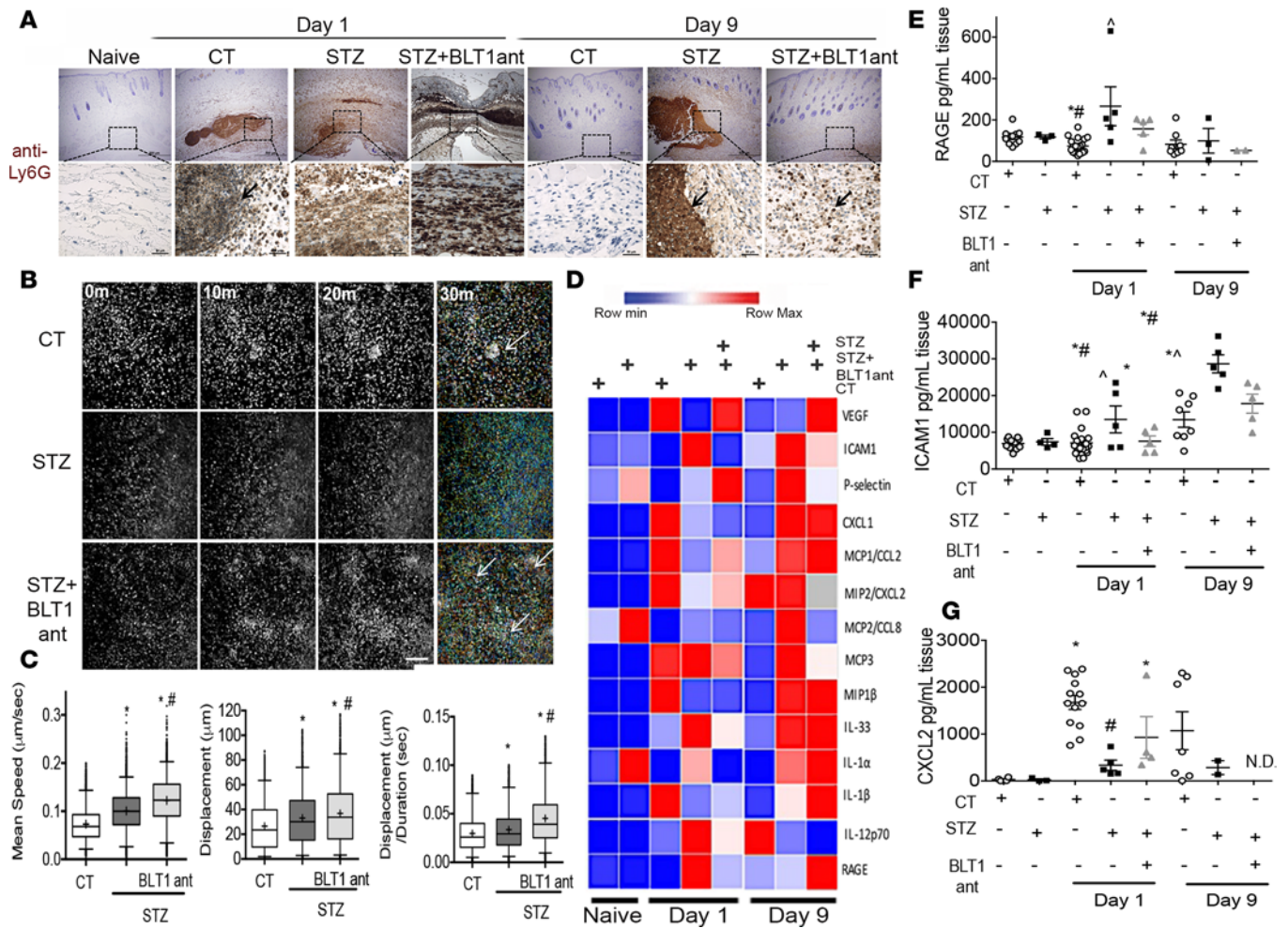


Figure 4. Excessive LTB_4 production drives poor neutrophil organization and altered chemokine/cytokine production at the site of infection of diabetic mice. (A) Biopsies were collected from CT and diabetic naive mice and infected mice, and they were treated daily with the BLT1 antagonist on days 1 and 9 after MRSA skin infection and sectioned for histology. Representative images of IHC for neutrophils (Ly6G/C) are stained in brown with blue counterstain from 3–5 mice from 2–4 experiments. Top panels show 4 \times magnification. Bottom panels show 40 \times magnification. Black arrows indicate neutrophils. (B) Intravital imaging from the infection site of Lys^{EGFP} CT and diabetic mice with frames taken at 0, 10, 20, and 30 minutes. The 30-minute frames include track paths of individual cells. The lines show the cell path and the color refers to the median velocity of the cell (red is fast, blue is slow). (C) Left graph: Median velocity of GFP^+ cells. Middle graph: Track displacement of GFP^+ cells. Right graph: Ratio of displacement/track duration to determine the directionality of GFP^+ cells. (D) Tissue homogenate from CT and diabetic mice that were infected or not and treated with the BLT1 antagonist once a day for 9 days were subjected to a multiplex assay, and the heatmap of analytes from 3–8 mice are shown. (E–G) Skin homogenates were processed and subjected to ELISA for RAGE, ICAM-1, and CXCL2 abundance. Data are mean \pm SEM of 3–8 mice from 2–4 experiments. * $P < 0.05$ vs. naive mice. # $P < 0.05$ vs. CT mice. ^ $P < 0.05$ vs. STZ mice treated with vehicle control ointment.

molecules detected (Figure 4, E–G). These data show that early production of LTB_4 contributes to induction of inflammatory cytokines but not chemokines during infection of diabetic mice and that, during late time points, LTB_4 might contribute to the tissue damage caused by IL-33 and IL-1 α .

Macrophages in diabetic mice are detrimental to host defense. Macrophages have been shown to surround the neutrophilic abscess (28). Furthermore, these cells are also involved in the production of inflammatory mediators involved in neutrophil migration and enhanced antimicrobial functions (29). Therefore, we investigated whether the diabetic milieu affected macrophage localization or activation. We detected F4/80 $^+$ macrophages in the skin at various time points after infection with MRSA by IHC. At day 1 after infection, macrophages in nondiabetic mice were localized along the periphery of the abscess, but in diabetic mice, macrophages were found in locations further from the abscess and in different areas of the skin, such as epidermis and adipose tissue (Figure 5A). BLT1 antagonist treatment restored the localization of macrophages to regions near the abscess and neutrophil aggregates. At day 9 after infection, nondiabetic mice exhibited a greater number of macrophages in the skin compared with control

uninfected skin. Interestingly, we detected a robust increase in macrophages in the skin of diabetic mice at day 9 after infection compared with the skin of infected nondiabetic mice, and this increase was substantially reduced with BLT1 antagonist treatment (Figure 5A). These data led to the hypothesis that alternate macrophage location and activation state is responsible for abnormal neutrophil migration, abscess formation, and detrimental MRSA skin host defense in diabetic mice.

To further examine the potential detrimental role of skin macrophages during MRSA skin infection in diabetic mice, we depleted macrophages prior to infection by using monocyte/macrophage diphtheria toxin receptor (MMDTR) mice. MMDTR mice contain a DTR-mCherry fluorescent fusion protein that is specifically expressed in monocytes and macrophages. Diabetic and nondiabetic MMDTR mice were treated with DT or the vehicle control to deplete macrophages prior to infection. We determined whether macrophages influence neutrophil migration to the site of infection in diabetic mice. Immunofluorescence analysis revealed more robust neutrophil recruitment 6 hours after infection in diabetic MMDTR mice compared with infected nondiabetic mice (Figure 5B). However, diabetic DT-treated MMDTR mice showed a decrease in neutrophil recruitment to the skin. At 2 days after infection, while diabetic MMDTR mice had a significantly larger infection area compared with nondiabetic MMDTR mice, DT-treated diabetic MMDTR mice exhibited a reduced infection area compared with vehicle-treated diabetic MMDTR mice (Figure 5C). These data correlated with the reduced bacterial burden (Figure 5D). Flow cytometry analysis of skin biopsies confirmed the observations that DT treatment reduced the numbers of Ly6G⁺ neutrophils in the skin at 6 hours after infection (Figure 5E). Macrophage depletion also decreased the levels of LTB₄ in the skin, suggesting that macrophages are either a significant source of LTB₄ or that these cells are needed to promote the production of LTB₄ (Figure 5F).

Next, we determined whether macrophage depletion altered production of inflammatory mediators in the skin using a multiplex assay. Macrophage depletion in diabetic MMDTR mice restored expression of many of the chemokines and cytokines to levels similar to those in nondiabetic mice. Depletion of macrophages in diabetic mice resulted in lowered expression of CXCL2 (Figure 5G) and CCL2 (Figure 5I); however, levels of P-selectin (Figure 5J) remained unchanged. Furthermore, expression of MMP8 was elevated in diabetic mice but reduced in diabetic mice without macrophages (Figure 5H). These results show that skin macrophages play a significant role in the production of inflammatory mediators that likely contribute to LTB₄-induced excessive inflammation and poor host defense in diabetic mice infected with MRSA.

Discussion

Skin infection is a common threat to people with diabetes. Although skin infection models shed light into the poor antimicrobial effector function and control of bacterial infection, the cellular interactions, behavior, and key molecules responsible for poor host defense in diabetic mice is poorly understood.

In the current study, we utilized state-of-the-art techniques, along with epistatic and gain-of-function experiments to address the question of whether aberrant LTB₄ drives poor host defense in diabetic mice. We observed that diabetic mice produce aberrantly high levels of the bioactive lipid mediator LTB₄ during MRSA skin infection, and this overexpression correlated with poor bacterial control, uncontrolled cell recruitment, and inefficient abscess development. Macrophages are likely players involved in promoting aberrant LTB₄ levels, as evidenced by the restoration of host defenses upon specific deletion of monocytes and macrophages in diabetic mice. Additionally, topical application of BLT1 but not BLT2 antagonist restored host defense in diabetic mice, as evidenced by a reduction in infection area, restriction of cell recruitment, and limited inflammation (Figure 6). Since skin infections in patients with diabetes are difficult to treat and often fail to heal, there is a great need for improved therapeutic strategies. Our results suggest that topical treatment with BLT1 antagonists offers a potential therapeutic approach to reduce abundant inflammation and restore host defense during MRSA skin infection in patients with diabetes.

In general, improved understanding of how diabetes alters immune functions may facilitate the development of new therapies to restore host defenses in this vulnerable population. Patients with diabetes are more susceptible to infections, leading to the initial hypothesis that these individuals produce lower levels of inflammatory mediators that promote host defense. However, many of these mediators, such as LTB₄, promote host defense mechanisms by boosting inflammation. Because diabetes is associated with chronic low-grade inflammation, the levels of inflammatory mediators are altered even in the absence of infection; however, the role of these inflammatory mediators in infections in diabetes patients remains unknown. Along with other inflammatory mediators, LTB₄ levels are higher in the serum of mice and patients with

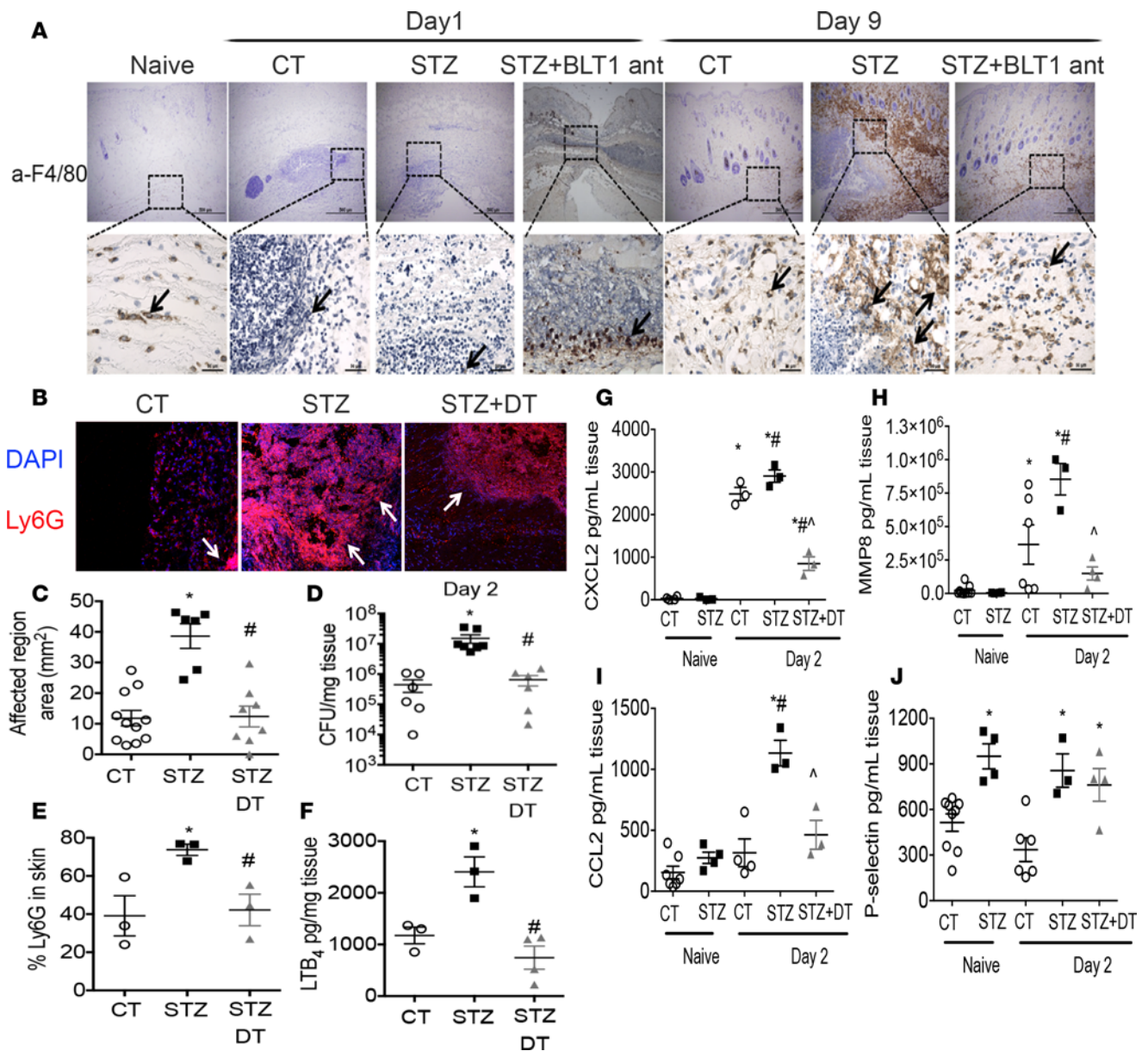


Figure 5. Skin-macrophages drive detrimental host defense actions in diabetic mice. (A) CT and STZ mice were infected and treated with the BLT1 antagonist once a day for 9 days, and skin biopsies from days 1 and 9 after infection were subjected to IHC staining for macrophages (F4/80) in brown with blue counterstain. Top panels show 40× magnification, and bottom panels show 400× magnification from 3–5 mice from 2–4 experiments. Arrows indicate macrophages. (B) Monocytes and macrophages were depleted in diabetic MMDTR mice as described in the Methods prior to MRSA skin infection. After 6 hours, skin biopsies were collected and sectioned for immunofluorescence staining for neutrophils (Ly6G) shown in red and DAPI counterstain shown in blue. Representative images of 20× magnification from 3–4 mice. White arrows indicate neutrophils. (C) Infection areas of CT, STZ, and DT-treated STZ-MMDTR mice on day 2 after infection with MRSA. (D) Bacterial CFU in the skin CT, STZ, and DT-treated STZ-MMDTR determined 2 days after infection. (E) Percentage of neutrophils (Ly6G⁺) in the skin of CT, STZ, and DT-treated STZ-MMDTR determined by flow cytometry at day 2 after infection. (F) LTB₄ ELISA on tissue homogenates detected 2 days after infection from CT, STZ, and DT-treated STZ-MMDTR mice. Data are mean ± SEM of 3–7 mice from 1–2 experiments. **P* < 0.05 vs. CT mice. #*P* < 0.05 vs. STZ-treated mice. (G–J) Multiplex assay on skin biopsy homogenates 2 days after infection of CT, STZ, and DT-treated STZ-MMDTR CXCL2 (G), MMP8 (H), CCL2 (I), and P-selectin (J). Data are mean ± SEM of 3–7 mice from 1–2 experiments. **P* < 0.05 vs. naive mice. #*P* < 0.05 vs. CT mice. ^*P* < 0.05 vs. STZ-treated mice.

diabetes (30). Phagocytes from patients with diabetes exhibit impaired function. Specifically, reduced respiratory burst and defective phagocytosis are associated with poor bacterial clearance. Immune cells from mice and rats with diabetes reportedly have poor phagocytosis and cytokine production (31–33). Furthermore, in patients with diabetes, neutrophils exhibit poor recruitment to the site of infection or injury, contributing to the patient's susceptibility to infections (34). Although LTB₄/BLT1 is important for naive

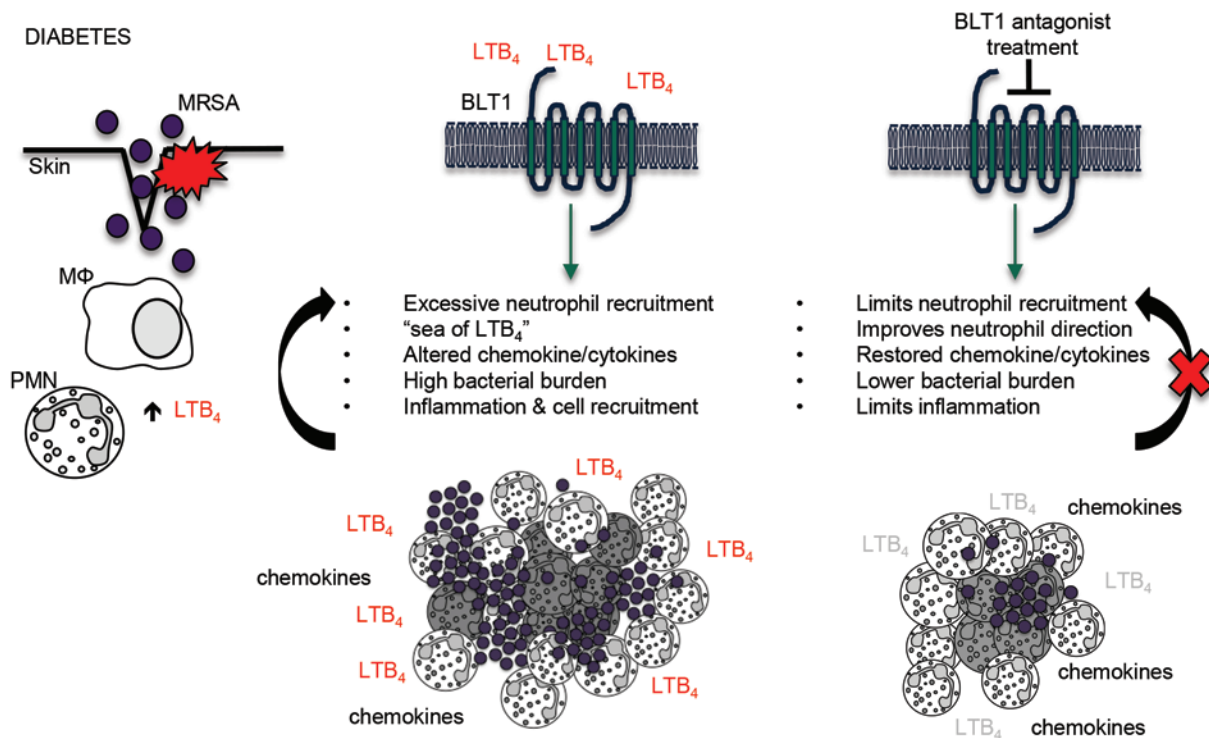


Figure 6. Summary. Left panel: MRSA skin infection induces macrophage activation, which leads to LTB₄ production and neutrophil recruitment. Both of these outcomes are elevated in diabetic animals compared with control animals. Middle panel: Excessive LTB₄/BLT1 activity in the skin during MRSA infection in diabetic mice results in uncontrolled neutrophil recruitment, poor abscess formation, uncontrolled bacterial burden, and exaggerated inflammation. Right panel: BLT1 antagonist treatment of infected diabetic mice results in reduced neutrophil recruitment, restoration of neutrophil direction, proper abscess formation, and improved bacterial clearance. Our model suggests that BLT1 antagonist treatment dampens the cycle of chronic inflammation during infection.

macrophages and neutrophils to phagocytose and kill pathogens (10, 15, 35), we found that BLT1 antagonism was associated with better bacterial clearance in diabetic mice. Because phagocytes from patients with diabetes have poor antimicrobial activity, it is unlikely that BLT1 antagonism impairs these functions in our model system. Instead, it is more likely that uncontrolled activation of other inflammatory programs, such as uncontrolled cytokine and chemokine production, may be the key driver of poor host defense in diabetic mice. Since diabetes is characterized by chronic inflammation, it is possible that excessive LTB₄/BLT1 signaling induces signaling cascades that incapacitate skin host defense. With this, BLT1 antagonist treatment in diabetic mice may restore the inflammatory signaling pathways that favor bacterial clearance.

Abscess formation during MRSA skin infection facilitates containment and eliminates bacteria, and thus, impaired abscess formation could result in dissemination of infections. Neutrophils in the skin of diabetic mice failed to assemble into an organized abscess. The factors involved in neutrophil swarming and abscess formation include LTB₄ and additional chemokines. The location of excessive LTB₄ in the skin of diabetic mice may contribute to poor neutrophil abscess formation. Because LTB₄ is a chemotactic molecule, excessive LTB₄ levels may disrupt chemoattractant gradients in the skin and impair directed chemotaxis. Blockade of BLT1 in diabetic mice restored neutrophil directional movement, possibly by restoring the balance among different chemotactic molecules or by allowing neutrophils to detect gradients of other chemokines in the skin. These events may allow for better abscess formation during MRSA skin infection to improve bacterial containment in diabetic mice.

During MRSA skin infection, macrophages were found close to the neutrophilic abscess. In uninfected naïve skin, no significant differences in the basal levels of LTB₄ or the numbers of macrophages in the skin were noted between diabetic and nondiabetic mice. However, during MRSA skin infection, high LTB₄ levels and dysregulated production of chemokines and cytokines were observed in diabetic mice. Interestingly, expression levels of *Alox5* were not significantly different in the skin of diabetic or nondiabetic mice

at day 1 after infection. Together, these findings suggest that 5-LO or other enzymes may be more active in the skin of diabetic mice during infection. Because diabetic mice depleted of macrophages (DT-treated diabetic MMDTR mice) showed significant improvement in host defense, it is likely that the activation of macrophages in diabetic skin contributes to excessive LTB_4 levels that are detrimental to host defense in the skin. However, it remains to be determined whether macrophage depletion at different time points throughout the course of infection is beneficial. Because macrophages restore homeostasis by eliminating apoptotic cells and promoting tissue remodeling, it is possible that macrophage depletion at later stages of infection may interfere with the resolution phase, negating the positive effect of macrophage depletion in early stages of infection.

The effects of BLT1 antagonist treatment on other cell types in the skin may also contribute to reducing inflammation during infection. Keratinocytes express BLT1, and because the BLT1 antagonist treatment ointments are applied topically, LTB_4 may also influence keratinocyte-induced cytokines and antimicrobial peptides (36). Additionally, keratinocytes from patients with diabetes have impaired cell migration and proliferation (37), and treatment with a BLT1 antagonist may alter the inflammatory profile of these cells, even in the absence of infection. Further experiments are needed to determine how the BLT1 antagonist influences other immune and nonimmune cells during infection or injury.

Although our data demonstrate that exaggerated LTB_4 production and uncontrolled BLT1 signaling are driving factors in poor host defense in diabetic mice, we cannot exclude the possibility that other inflammatory mediators are also involved in poor host defense during MRSA skin infection in diabetic mice. While BLT1 antagonist treatment improves host defense in diabetic mice, we also detected elevated levels of chemokines and cytokines, such as CXCL2, MCP3, and IL-33, which were not inhibited by BLT1 antagonist treatment. Therefore, it remains to be determined whether these molecules are also detrimental to skin host defense in diabetes.

Although previous reports have indicated that leukocytes in mice do not express BLT2, we and others have detected BLT2 expression in murine phagocytes (38, 39); however, the role of this molecule in host defense is not well understood. Blockade of BLT2 does not influence phagocytosis and killing of *Streptococcus pyogenes* by alveolar macrophages (35); however, blockade of BLT2 in BM-derived macrophages impairs phagocytosis of *Borrelia burgdorferi* (39). Thus, it is possible that BLT1 antagonism in diabetic mice may allow for LTB_4 /BLT2 activity to facilitate phagocytosis, but our data show that pharmacological BLT2 blockade did not improve skin host defense in diabetic mice (Figure 2, C and D). Whether blockade of both BLT1 and BLT2 receptors further enhances host defense in diabetic mice is unknown at this time. Furthermore, other lipid mediators have higher affinity than LTB_4 for BLT2. BLT2 plays a beneficial role in skin wound healing via the activity of 12-hydroxyheptadecatrienoic acid (12-HHT), which mediate TNF- α and MMP production (40). In fact, 12-HHT has been shown to be essential for keratinocyte wound healing in diabetic mice (41). Additionally, 12-HETE and BLT2 effects have been found to be necessary for enhancing VEGF expression and promoting wound healing (42). While we detected lower levels of 12-HETE in the infected skin of diabetic mice at day 1, this expression of this eicosanoid was significantly elevated at day 9 after MRSA skin infection in diabetic mice. Interestingly, other HETE products showed a different expression pattern during infection in diabetic and nondiabetic mice. We did not detect differences in 5-HETE between diabetic and nondiabetic mice, but the antiinflammatory HETES (12-HETE and 15-HETE) were substantially decreased at day 1 and increased at day 9 after infection in diabetic mice. We only observed the increased production of 8-HETE in the naive skin of diabetic mice. Whether these lipids play a differential role in host defense in the skin of diabetic mice remains to be determined. Although other lipid mediators are beneficial to wound healing responses through BLT2 signaling, less is known about specific LTB_4 /BLT2 effects on phagocyte effector functions during infections. Such events are of interest and will be studied in imminent future work.

Due to the pleiotropic effects of LTB_4 , blockade of BLT1 activity restored many detrimental aspects in skin lesion in diabetic mice. Specifically, BLT1 blockade resulted in increased neutrophil recruitment, improved abscess formation, decreases in exaggerated cytokine/chemokine production, and lessened tissue injury. Based on our findings, novel treatment strategies could include cotherapy with antibiotics and BLT1 blockade to promote a faster infection clearance. Cases of antibiotic-resistant infections are expected to rise without the development of new treatment strategies, and patients with diabetes represent one of the many patient populations that are at higher risk for infections. Reduction of skin inflammation via topical BLT1 antagonism therapy, therefore, holds potential for clinical restoration of host defense and improved patient outcome.

Methods

Study design. The goal of the study was to determine the impact of chronic LTB₄/BLT1 actions on poor host defense to MRSA skin infection in diabetic mice. WT and transgenic mice were used in experiments along with pharmacological inhibition. Experiments included a s.c. infection model coupled with intravital microscopy, multiplex measurement of inflammatory mediators, IVIS (PerkinElmer), histological analysis, and flow cytometry analysis. Sample sizes were determined using a power and sample size calculator (<http://www.statisticssolutions.com/>) to measure group mean differences of 2 times the observed standard error with a power of 0.8 and significance of 0.05. Sample sizes averaged 5–10 animals per group. Samples were randomized but not blinded.

Mouse strains. Mice were purchased from the Jackson Laboratory or were donated from other investigators. *Lys^{EGFP}* (B6.129(Cg)-*Lyz2^{mi.1Graf}/Mmmh*) mice (43) were a gift from Nadia Carlesso (City of Hope, Duarte, California, USA), and pIL1DsRED mice were a gift from Akiko Takashima (University of Toledo, Toledo, Ohio, USA; ref. 44). C57BL/6J, BLT1^{-/-} (B6.129S4-*Ltb4r1^{miAdl}/J*) and *5-LO^{-/-}* (B6.129S2-*Alox5^{miFun}/J*) mouse colonies were initially obtained from the Jackson Laboratory and maintained by breeding homozygous KO brother-sister mating pairs to sustain homozygosity.

MMDTR mice or *Csfr1^{LsL-DTR-mCherry} LysM^{cre}* were used to specifically deplete monocytes and macrophages (45). *Csfr1^{LsL-DTR-mCherry}* mice were bred with *LysM^{cre}* (B6.129-*Lyzs^{mi(cre)Jfo}/J*) mice to allow for expression of the DTR-mCherry fusion protein. MMDTR mice allowed for the detection of monocytes/macrophages by mCherry fluorescence and for specific cell ablation when mice were treated with DT. Mice containing the floxed stop codon-DTR-mCherry construct, but lacking Cre expression, were used as controls.

Induction of diabetes. For the STZ-induced diabetes model, 6- to 8-week-old male C57BL/6J mice were treated by i.p. injection with 40 mg/kg of STZ (Adipogen) dissolved in 0.1 M sodium citrate buffer once daily for 5 consecutive days (46, 48). Female mice were not used since female mice are more resistant to developing hyperglycemia following STZ treatment (49). Nondiabetic control mice received citrate buffer and served as a vehicle control. Mice were considered diabetic when blood glucose levels were >250 mg/dl. Mice were treated with STZ to induce diabetes 30 days prior to MRSA skin infection. Since both *Alox5^{-/-}* and *Ltb4r1^{-/-}* mice were more resistant to developing hyperglycemia after STZ treatment, these KO mice were treated with 3–5 additional injections of 40 mg/kg of STZ to achieve hyperglycemia. Age-matched WT and KO mice with similar blood glucose levels were used for experiments.

NOD mice were maintained at Indiana University School of Medicine. Starting at 10 weeks of age, blood glucose levels were monitored weekly in female NOD mice using an OneTouch Ultra (LifeScan) glucose meter and strips. When blood glucose levels reached 250 mg/dl, mice were considered diabetic (dbNOD, ref. 47). Age-matched female NOD mice that did not become diabetic (glucose levels <150 mg/dl) were used as controls (ctNOD). Once NOD mice became diabetic, they were used in experiments within 1–2 weeks. Body weight was monitored, and mice that lost more than 20% of their original body weight were excluded from experimentation. NOD mice were approximately 12–20 weeks of age at the time of MRSA skin infection.

MRSA strains. The MRSA USA300 LAC strain was a gift from Bethany Moore (University of Michigan, Ann Arbor, Michigan, USA; ref. 50). The bioluminescent USA300 (NRS384 lux) strain was a gift from Roger Plaut (Food and Drug Administration, Silver Spring, Maryland, USA; ref. 51). The GFP-expressing USA300 strain was a gift from William Nauseef (University of Iowa, Iowa City, Iowa; ref. 52). MRSA stocks were stored at -80°C. MRSA was cultured as previously described (53).

MRSA skin infection. The murine skin infection model was adapted from a previous study (54). Male mice between 6 and 12 weeks of age were used for MRSA skin infection. Mice were infected with approximately 3 × 10⁶ MRSA, and biopsies and sample collection were taken at various times, ranging from 6 hours to 9 days after infection, as previously described (53).

Ointment preparation. Ointments were prepared by emulsifying the active ingredient into 100% petroleum jelly (Vaseline) daily prior to treatment application. Treatments were applied to cover the infected area with a clean cotton swab. Mice were treated once a day throughout the course of infection as indicated.

Two-photon intravital microscopy imaging. Mice were infected with MRSA and were anesthetized with a mixture of ketamine and xylazine, and a skin flap was created surrounding the infection area as described (55). The skin flap was placed in a coverslip-bottomed cell culture dish for imaging and moistened with PBS. Mice were imaged for up to 1 hour. Imaging was performed using an Olympus FV1000-MPE confocal/multiphoton microscope. While still anesthetized, mice were euthanized

immediately after imaging. The analysis was performed using FIJI (ImageJ) tracking software using the TrackMate plugin.

In vivo imaging with IVIS. An IVIS Spectrum/CT (Perkin Elmer) in vivo optical instrument was used to image both bioluminescence and fluorescence in the mice. Mice were induced with 3%–5% isoflurane (balance medical oxygen) and anesthesia maintained with 1%–2% isoflurane during the entire imaging period. Mice were positioned on a heated platform (37°C) facing the CCD camera and imaged for the appropriate bioluminescence/fluorescence (see below).

Bioluminescence imaging (BLI) and analysis. Up to 5 mice were simultaneously scanned without filtration for between 0.5–4 minutes to allow for a sufficient bioluminescent signal to be accumulated by the instrument (IVIS Spectrum/CT, Perkin Elmer). Mice were scanned temporally over the course of the MRSA skin infection. To quantify the degree of MRSA infection, a region of interest was manually drawn around each infection, and total flux (photons/sec) was measured for each infection site. In addition, a background region was also examined to permit subtraction of ambient scattered photons that were not associated with bacterial emission. To obtain the background-free total flux signal, the mouse infection region was subtracted from the background region. To establish the relationship between bacterial CFU and background-free total photon flux, a standard curve was created for each infection. The standard curve was prepared by spotting known bacterial CFU on TSA plates (in vitro) or infecting mice s.c. with known bacterial CFU (in vivo) followed by imaging. A plot of bioluminescence background-free total flux (y axis) and CFU (x axis) was generated, and from this relationship, estimates of bacterial burden in the skin could be computed.

DsRed and mCherry scans and analysis. WT mice that were DsRed-negative (or mCherry-negative) served as the autofluorescence background controls. For DsRed and mCherry fluorescence imaging, in the presence of bioluminescent MRSA, groups of 4 mice were imaged at 6–8 distinct emission wavelengths over the (excitation: 535, 570, 605 nm) 560–680 nm and (excitation: 500, 535, 570 nm) 580–720 nm bandwidths, respectively, with an exposure range of 1–5 sec/group. To provide negative controls, WT mice that were DsRed-negative (or mCherry-negative) with and without bioluminescent MRSA were imaged as above and served as bioluminescent MRSA and autofluorescence controls, respectively. Because the total emission in each mouse is a linear combination of DsRed (or mCherry) fluorescence combined with MRSA bioluminescence, the fluorescence emission must be spectrally deconvolved. Individual basis functions for each spectral series were constructed as follows:

$$E_{AUTO}(\lambda, i) = E_{WT}$$

$$E_{BL}(\lambda, i) = E_{MRSA}(\lambda, i) - E_{AUTO}(\lambda, i)$$

$$E_{FL}(\lambda, i) = E_{TOTAL}(\lambda) - E_{BL}(\lambda, i)$$

Where $\lambda, i, E_{AUTO}, E_{WT}, E_{BL}, E_{MRSA}, E_{TOTAL}$, and E_{FL} are the wavelength, subject, autofluorescence emission, WT emission (i.e., no DsRed or mCherry), bioluminescence emission, MRSA emission (i.e., bioluminescence + autofluorescence), total emission (i.e., bioluminescence + autofluorescence + DsRed or mCherry), and DsRed (or mCherry) emission, respectively. Wavelength-dependent spectral basis functions were manually constructed and loaded into LivingImage (PerkinElmer), where DsRed (or mCherry) spatially dependent signals for each pixel were spectrally deconvolved using a multilinear least-squares approach. Once the images were spectrally decomposed, a region of interest was drawn around the DsRed (or mCherry) signal, and the average pixel intensity was reported in total radiant efficiency ([photons/second]/[$\mu\text{W}/\text{cm}^2$]).

Skin dissociation and flow cytometry. Skin biopsy sections were digested with 1 mg/ml collagenase-D (Roche Diagnostics) for 3 hours at 37°C in 1 ml DMEM. Reactions were quenched with EDTA at a final concentration of 10 mM. Tissue sections were passed through a 70- μm cell strainer and washed with PBS. Single cells were stained with fluorescent antibodies or dyes for flow cytometry analysis on the BD LSR II flow cytometer. Analyses were performed using FlowJo software. The following antibodies were utilized: BLT1-PE (BD Biosciences; catalog 552836; clone 203/14F11), BLT2-AF647 (Bioss; catalog bs-2655R-A647; polyclonal), Ly6G-AF488 (BioLegend; catalog 127626; clone 1A8), Ly6G-PerCPCy5.5 (BioLegend; catalog 127616; clone 1A8), F4/80-PE (BioLegend; catalog 123110; clone BM8), F4/80-AF700 (BioLegend; catalog 123130; clone BM8), CD45-Pacific blue (BioLegend; catalog 103126; clone 30-F11), mouse CD16/32 Fc blocking antibody (BioLegend; catalog 101320; clone 93), and Zombie UV viability dye (BioLegend; catalog 423107).

MMDTR mice and macrophage depletion. To deplete macrophages, MMDTR mice were treated with 100 ng DT or PBS vehicle control once a day for 3 consecutive days prior to MRSA skin infection. Skin biopsy punches were collected at 6 hours or day 1 after MRSA skin infection.

Sample preparation for MS. Skin biopsy sections were collected and flash frozen with dry ice. Samples were processed by the Vanderbilt University Eicosanoid Core Laboratory as previously described (56). Briefly, skin samples were homogenized and extracted in ice-cold methanol with indomethacin and butylated hydroxytoluene (BHT). Samples were then injected for liquid chromatography-MS (LC-MS). Eicosanoids were identified and quantified based on the mass and amount of known standards as previously described (56).

Statistics. Data analysis was performed in GraphPad Prism software. Statistical tests used are listed for each experiment in the corresponding figure legends. Briefly, Student's 2-tailed *t* tests were used to compare 2 experimental groups. One-way ANOVA followed by Tukey's multiple comparison corrections was used to compare 3 or more groups. Two-way ANOVA with repeated measured followed by Tukey's multiple comparison corrections was used to compare infection areas over time between 2 or more mouse groups. *P* < 0.05 was considered statistically significant.

Study approval. Experiments were performed at Indiana University School of Medicine in Indianapolis, and/or at Vanderbilt University Medical Center under the guidance of the IACUC at Indiana University and/or Vanderbilt University Medical Center, and all experimental procedures were approved prior to conducting studies.

Author contributions

SLB and CHS designed the experiments and analyzed data. SLB, SW, NND, and NK performed the experiments. LF, SW, BPM, and PRT assisted with experiments and analyzed data. SLB and CHS wrote the manuscript.

Acknowledgments

We thank Nadia Carlesso (City of Hope, Duarte, California, USA) for providing the *Lys^{EGFP}* mice. We thank Bethany Moore (University of Michigan, Ann Arbor, Michigan, USA) for providing the MRSA USA300 LAC strain and Roger Plaut (Food and Drug Administration, Silver Spring, Maryland, USA) for providing the bioluminescent USA300 (NRS384 lux) MRSA strain. This work was supported by NIH grants HL-103777 and R01HL124159-01 (to CHS) and T32AI060519 (to SLB).

Address correspondence to: C. Henrique Serezani, Vanderbilt University Medical Center, Department of Infectious Diseases, 1161 21st Avenue South, MCN A2310A, Nashville, Tennessee 37232, USA. Phone: 615.875.8626; Email: h.serezan@vanderbilt.edu.

SLB's present address is: Department of Pediatrics, University of California San Diego, La Jolla, California, USA.

1. Wild S, Roglic G, Green A, Sicree R, King H. Global prevalence of diabetes: estimates for the year 2000 and projections for 2030. *Diabetes Care*. 2004;27(5):1047–1053.
2. Casqueiro J, Casqueiro J, Alves C. Infections in patients with diabetes mellitus: A review of pathogenesis. *Indian J Endocrinol Metab*. 2012;16 Suppl 1:S27–S36.
3. Muller LM, et al. Increased risk of common infections in patients with type 1 and type 2 diabetes mellitus. *Clin Infect Dis*. 2005;41(3):281–288.
4. Lipsky BA, Tabak YP, Johannes RS, Vo L, Hyde L, Weigelt JA. Skin and soft tissue infections in hospitalised patients with diabetes: culture isolates and risk factors associated with mortality, length of stay and cost. *Diabetologia*. 2010;53(5):914–923.
5. Driver VR, Fabbi M, Lavery LA, Gibbons G. The costs of diabetic foot: the economic case for the limb salvage team. *J Am Podiatr Med Assoc*. 2010;100(5):335–341.
6. Ki V, Rotstein C. Bacterial skin and soft tissue infections in adults: A review of their epidemiology, pathogenesis, diagnosis, treatment and site of care. *Can J Infect Dis Med Microbiol*. 2008;19(2):173–184.
7. Miller LS, Cho JS. Immunity against *Staphylococcus aureus* cutaneous infections. *Nat Rev Immunol*. 2011;11(8):505–518.
8. Kobayashi SD, Malachowa N, DeLeo FR. Pathogenesis of *Staphylococcus aureus* abscesses. *Am J Pathol*. 2015;185(6):1518–1527.
9. Canetti C, Hu B, Curtis JL, Peters-Golden M. Syk activation is a leukotriene B4-regulated event involved in macrophage phagocytosis of IgG-coated targets but not apoptotic cells. *Blood*. 2003;102(5):1877–1883.
10. Mancuso P, Nana-Sinkam P, Peters-Golden M. Leukotriene B4 augments neutrophil phagocytosis of *Klebsiella pneumoniae*. *Infect Immun*. 2001;69(4):2011–2016.

11. Secatto A, et al. 5-Lipoxygenase deficiency impairs innate and adaptive immune responses during fungal infection. *PLoS One*. 2012;7(3):e31701.
12. Secatto A, et al. The leukotriene B₄/BLT₁ axis is a key determinant in susceptibility and resistance to histoplasmosis. *PLoS One*. 2014;9(1):e85083.
13. Serezani CH, Kane S, Collins L, Morato-Marques M, Osterholzer JJ, Peters-Golden M. Macrophage dectin-1 expression is controlled by leukotriene B₄ via a GM-CSF/PU.1 axis. *J Immunol*. 2012;189(2):906–915.
14. Santos PC, et al. The pivotal role of 5-lipoxygenase-derived LTB₄ in controlling pulmonary paracoccidioidomycosis. *PLoS Negl Trop Dis*. 2013;7(8):e2390.
15. Morato CI, et al. Essential role of leukotriene B₄ on Leishmania (Viannia) braziliensis killing by human macrophages. *Microbes Infect*. 2014;16(11):945–953.
16. Tavares NM, et al. Understanding the mechanisms controlling Leishmania amazonensis infection in vitro: the role of LTB₄ derived from human neutrophils. *J Infect Dis*. 2014;210(4):656–666.
17. Montuschi P, Kharitonov SA, Ciabattini G, Barnes PJ. Exhaled leukotrienes and prostaglandins in COPD. *Thorax*. 2003;58(7):585–588.
18. Chen M, et al. Neutrophil-derived leukotriene B₄ is required for inflammatory arthritis. *J Exp Med*. 2006;203(4):837–842.
19. Martínez-Clemente M, Clària J, Titos E. The 5-lipoxygenase/leukotriene pathway in obesity, insulin resistance, and fatty liver disease. *Curr Opin Clin Nutr Metab Care*. 2011;14(4):347–353.
20. Tobin DM, et al. The lta4h locus modulates susceptibility to mycobacterial infection in zebrafish and humans. *Cell*. 2010;140(5):717–730.
21. Filgueiras LR, et al. Leukotriene B₄-mediated sterile inflammation promotes susceptibility to sepsis in a mouse model of type 1 diabetes. *Sci Signal*. 2015;8(361):ra10.
22. Serreze DV, Gaedeke JW, Leiter EH. Hematopoietic stem-cell defects underlying abnormal macrophage development and maturation in NOD/Lt mice: defective regulation of cytokine receptors and protein kinase C. *Proc Natl Acad Sci USA*. 1993;90(20):9625–9629.
23. Serreze DV, Gaskins HR, Leiter EH. Defects in the differentiation and function of antigen presenting cells in NOD/Lt mice. *J Immunol*. 1993;150(6):2534–2543.
24. Pearson T, et al. Genetic separation of the transplantation tolerance and autoimmune phenotypes in NOD mice. *Rev Endocr Metab Disord*. 2003;4(3):255–261.
25. Cheng AG, DeDent AC, Schneewind O, Missiakas D. A play in four acts: Staphylococcus aureus abscess formation. *Trends Microbiol*. 2011;19(5):225–232.
26. Rådmark O, Werz O, Steinhilber D, Samuelsson B. 5-Lipoxygenase: regulation of expression and enzyme activity. *Trends Biochem Sci*. 2007;32(7):332–341.
27. Malachowa N, et al. Contribution of Staphylococcus aureus Coagulases and Clumping Factor A to Abscess Formation in a Rabbit Model of Skin and Soft Tissue Infection. *PLoS One*. 2016;11(6):e0158293.
28. Kienle K, Lämmermann T. Neutrophil swarming: an essential process of the neutrophil tissue response. *Immunol Rev*. 2016;273(1):76–93.
29. Schiwon M, et al. Crosstalk between sentinel and helper macrophages permits neutrophil migration into infected uroepithelium. *Cell*. 2014;156(3):456–468.
30. Parlapiano C, et al. The relationship between glycated hemoglobin and polymorphonuclear leukocyte leukotriene B₄ release in people with diabetes mellitus. *Diabetes Res Clin Pract*. 1999;46(1):43–45.
31. Foss NT, Foss-Freitas MC, Ferreira MA, Cardili RN, Barbosa CM, Foss MC. Impaired cytokine production by peripheral blood mononuclear cells in type 1 diabetic patients. *Diabetes Metab*. 2007;33(6):439–443.
32. Geerlings SE, Hoepelman AI. Immune dysfunction in patients with diabetes mellitus (DM). *FEMS Immunol Med Microbiol*. 1999;26(3-4):259–265.
33. Lecube A, Pachón G, Petriz J, Hernández C, Simó R. Phagocytic activity is impaired in type 2 diabetes mellitus and increases after metabolic improvement. *PLoS One*. 2011;6(8):e23366.
34. Alba-Loureiro TC, et al. Neutrophil function and metabolism in individuals with diabetes mellitus. *Braz J Med Biol Res*. 2007;40(8):1037–1044.
35. Soares EM, Mason KL, Rogers LM, Serezani CH, Faccioli LH, Aronoff DM. Leukotriene B₄ enhances innate immune defense against the puerperal sepsis agent Streptococcus pyogenes. *J Immunol*. 2013;190(4):1614–1622.
36. Braff MH, Di Nardo A, Gallo RL. Keratinocytes store the antimicrobial peptide cathelicidin in lamellar bodies. *J Invest Dermatol*. 2005;124(2):394–400.
37. Lan CC, Liu IH, Fang AH, Wen CH, Wu CS. Hyperglycaemic conditions decrease cultured keratinocyte mobility: implications for impaired wound healing in patients with diabetes. *Br J Dermatol*. 2008;159(5):1103–1115.
38. Lee AJ, Cho KJ, Kim JH. MyD88-BLT2-dependent cascade contributes to LPS-induced interleukin-6 production in mouse macrophage. *Exp Mol Med*. 2015;47:e156.
39. Zhang Y, Olson RM, Brown CR. Macrophage LTB₄ drives efficient phagocytosis of Borrelia burgdorferi via BLT1 or BLT2. *J Lipid Res*. 2017;58(3):494–503.
40. Yokomizo T. Two distinct leukotriene B₄ receptors, BLT1 and BLT2. *J Biochem*. 2015;157(2):65–71.
41. Liu M, et al. 12-Hydroxyheptadecatrienoic acid promotes epidermal wound healing by accelerating keratinocyte migration via the BLT2 receptor. *J Exp Med*. 2014;211(6):1063–1078.
42. Kim GY, Lee JW, Cho SH, Seo JM, Kim JH. Role of the low-affinity leukotriene B₄ receptor BLT2 in VEGF-induced angiogenesis. *Arterioscler Thromb Vasc Biol*. 2009;29(6):915–920.
43. Faust N, Varas F, Kelly LM, Heck S, Graf T. Insertion of enhanced green fluorescent protein into the lysozyme gene creates mice with green fluorescent granulocytes and macrophages. *Blood*. 2000;96(2):719–726.
44. Matsushima H, Ogawa Y, Miyazaki T, Tanaka H, Nishibu A, Takashima A. Intravital imaging of IL-1β production in skin. *J Invest Dermatol*. 2010;130(6):1571–1580.
45. Schreiber HA, et al. Intestinal monocytes and macrophages are required for T cell polarization in response to Citrobacter

- rodentium. *J Exp Med*. 2013;210(10):2025–2039.
46. Leiter EH. Multiple low-dose streptozotocin-induced hyperglycemia and insulinitis in C57BL mice: influence of inbred background, sex, and thymus. *Proc Natl Acad Sci USA*. 1982;79(2):630–634.
47. Diabetic Complications Consortium. Low-Dose Streptozotocin Induction Protocol (Mouse). DiaComp. <https://www.diacomp.org/shared/showFile.aspx?doctypeid=3&docid=19>. Accessed August 15, 2018.
48. Deeds MC, et al. Single dose streptozotocin-induced diabetes: considerations for study design in islet transplantation models. *Lab Anim*. 2011;45(3):131–140.
49. Makino S, Kunimoto K, Muraoka Y, Mizushima Y, Katagiri K, Tochino Y. Breeding of a non-obese, diabetic strain of mice. *Jikken Dobutsu*. 1980;29(1):1–13.
50. Domingo-Gonzalez R, Katz S, Serezani CH, Moore TA, Levine AM, Moore BB. Prostaglandin E2-induced changes in alveolar macrophage scavenger receptor profiles differentially alter phagocytosis of *Pseudomonas aeruginosa* and *Staphylococcus aureus* post-bone marrow transplant. *J Immunol*. 2013;190(11):5809–5817.
51. Plaut RD, Mocca CP, Prabhakara R, Merkel TJ, Stibitz S. Stably luminescent *Staphylococcus aureus* clinical strains for use in bioluminescent imaging. *PLoS One*. 2013;8(3):e59232.
52. Greenlee-Wacker MC, Rigby KM, Kobayashi SD, Porter AR, DeLeo FR, Nauseef WM. Phagocytosis of *Staphylococcus aureus* by human neutrophils prevents macrophage efferocytosis and induces programmed necrosis. *J Immunol*. 2014;192(10):4709–4717.
53. DeJani NN, et al. Topical Prostaglandin E Analog Restores Defective Dendritic Cell-Mediated Th17 Host Defense Against Methicillin-Resistant *Staphylococcus Aureus* in the Skin of Diabetic Mice. *Diabetes*. 2016;65(12):3718–3729.
54. Malachowa N, Kobayashi SD, Braughton KR, DeLeo FR. Mouse model of *Staphylococcus aureus* skin infection. *Methods Mol Biol*. 2013;1031:109–116.
55. Liese J, Rooijakkers SH, van Strijp JA, Novick RP, Dustin ML. Intravital two-photon microscopy of host-pathogen interactions in a mouse model of *Staphylococcus aureus* skin abscess formation. *Cell Microbiol*. 2013;15(6):891–909.
56. Timmons BC, et al. Prostaglandins are essential for cervical ripening in LPS-mediated preterm birth but not term or antiprogesterin-driven preterm ripening. *Endocrinology*. 2014;155(1):287–298.